The Astronomical Journal, 163:278 (11pp), 2022 June https://doi.org/10.3847/1538-3881/ac63c3
© 2022. The Author(s). Published by the American Astronomical Society.
OPEN ACCESS

Mapping out the Stellar Populations of IC 2602 and IC 2391

Azmain H. Nisak, Russel J. White, Alexandra Yep, Todd J. Henry, Leonardo Paredes, Hodari-Sadiki James, and Wei-Chun Jao
Astronomy Department, Georgia State University, Atlanta, GA 30303, USA; nisak@astro.gsu.edu, white@astro.gsu.edu
Received 2021 August 2; revised 2022 February 23; accepted 2022 February 24; published 2022 May 19

Abstract

IC 2391 and IC 2602 are important benchmarks for testing early star and planet evolution theories, both structural and dynamical, because they are the nearest open clusters with ages of ∼50 Myr. We refine membership lists for these clusters by identifying candidate members using Gaia DR2 kinematic and distance information. We identify 451 candidate members of IC 2602 and 350 candidate members of IC 2391. If confirmed, this would increase the known populations of these clusters by 275% and 130%, respectively. We use CHIRON on the CTIO/SMARTS 1.5 m telescope via fiber mode which yields a resolution of 27,400 to acquire high-resolution spectra of 26 new candidate cluster members brighter than $G = 13$ magnitude, as well as an additional 12 previously known members. Measures of lithium, Hα, stellar properties ($T_{\rm eff}$, log(g), [Fe/H]), radial velocities, and $v \sin i$ values from these spectra are used to confirm cluster membership. We find that 37 of 38 stars we observe are bona fide cluster members, of which four are new candidate photometric binaries and 10 are new candidate spectroscopic binaries.

Unified Astronomy Thesaurus concepts: Open star clusters (1160); Young star clusters (1833)

Supporting material: machine-readable tables

1. Introduction

IC 2602 and IC 2391are nearby (∼150 pc; Bravi et al. 2018) open clusters located in the Carina and Vela constellations respectively. Despite being spatially close on the sky (within 30°), the clusters differ in their space motions and likely do not share a common origin; the mean radial velocities of IC 2602 and IC 2391 are estimated to be 17.4 ± 1.0 km s^{-1} (Marsden et al. 2009) and 14.8 ± 0.7 km s^{-1} (Platais et al. 2007), respectively. It is believed that IC 2602 formed in conjunction with the Local association, otherwise known as the Pleaides supercluster (Eggen 1975, 1983a, 1983b), while IC 2391 formed alongside the Argus association (Torres et al. 2008; De Silva et al. 2013) as part of the IC 2391 supercluster (Eggen 1991). IC 2602 and IC 2391 experience low reddening with estimated $E(B - V)$ values of 0.068 ± 0.025 and 0.088 ± 0.027, respectively.

Spectra of their main-sequence FGK stars reveal that IC 2602 and IC 2391 have near-solar metallicities of 0.00 ± 0.01 and 0.06 ± 0.06 respectively (Randich et al. 2001, 2002; Platais et al. 2007; Boudreault & Bailer-Jones 2009; D'Orazi & Randich 2009; Marsden et al. 2009; Spina et al. 2017). Age estimates for IC 2602 and IC 2391are determined to be $43.7^{+4.3}_{-3.9}$ and $51.3^{+5.0}_{-4.5}$ Myr, respectively, which are inferred by modeling the lithium depletion boundary and chasm (Barrado y Navascués et al. 2004; Dobbie et al. 2010; Bravi et al. 2018). The age estimates are consistent with those determined from the main-sequence turnoff (∼30–50 Myr), which is potentially plagued by rapid rotation and gravity darkening (Brandt & Huang 2015; Jones et al. 2015; Cummings et al. 2017; Randich et al. 2018).

Given their close proximity and age, IC 2602 and IC 2391 are important benchmark clusters because they are the closest clusters with ages intermediate between that of star-forming regions (<10 Myr) and that of well-studied open clusters (>100 Myr; Lada & Lada 2003). At these transitional ages, low-mass stars are still gravitationally settling toward the main sequence (Baraffe et al. 2015) and planetary systems are in the process of dynamically evolving (Quinn & White 2016; Gaidos et al. 2017; Mann et al. 2017; Ragusa et al. 2018).

To study these clusters in detail, a plethora of investigations have been undertaken to identify potential candidate members of IC 2602 and IC 2391 via parallax, proper motion, spatial extent, and photometry (Feinstein 1961; Whiteoak 1961; Braes 1962; Lynga 1962; Foster et al. 1997; Rolleston & Byrne 1997; Simon & Patten 1998; Barrado y Navascués et al. 2001; Dodd 2004; Randich et al. 2005; Gagné et al. 2018). Additionally, numerous spectroscopic studies have been conducted to confirm candidate members via signatures of youth (e.g., lithium, Hα, large $v \sin i$) and stellar properties consistent with those of bona fide cluster members (Buscombe 1965; Abt & Morgan 1972; Levato et al. 1988; Messina et al. 2003; Paulson & Yelda 2006; Platais et al. 2007; Mermilliod et al. 2009; De Silva et al. 2013; D'Orazi et al. 2017; Merle et al. 2017). Both clusters appear to harbor a population of brown dwarfs (Barrado y Navascués et al. 2004; Dobbie et al. 2010).

The European Space Agency's Gaia satellite has revolutionized our capacity to recognize and characterize Galactic star clusters and has the potential to significantly refine membership lists for open clusters (Cantat-Gaudin et al. 2018; Lodieu et al. 2019; Zuckerman et al. 2019). However, while the Gaia Collaboration's prescription is largely successful in identifying candidate cluster members (Gaia Collaboration et al. 2018), the prescription is still known to miss bona fide members in some instances (Zuckerman et al. 2019). Furthermore, stars retrieved from Gaia are still only candidate members until confirmed with spectra because even the best samples are affected by contamination from field stars (Briceno et al. 2019).

Original content from this work may be used under the terms of the Creative Commons Attribution 4.0 licence. Any further distribution of this work must maintain attribution to the author(s) and the title of the work, journal citation and DOI.

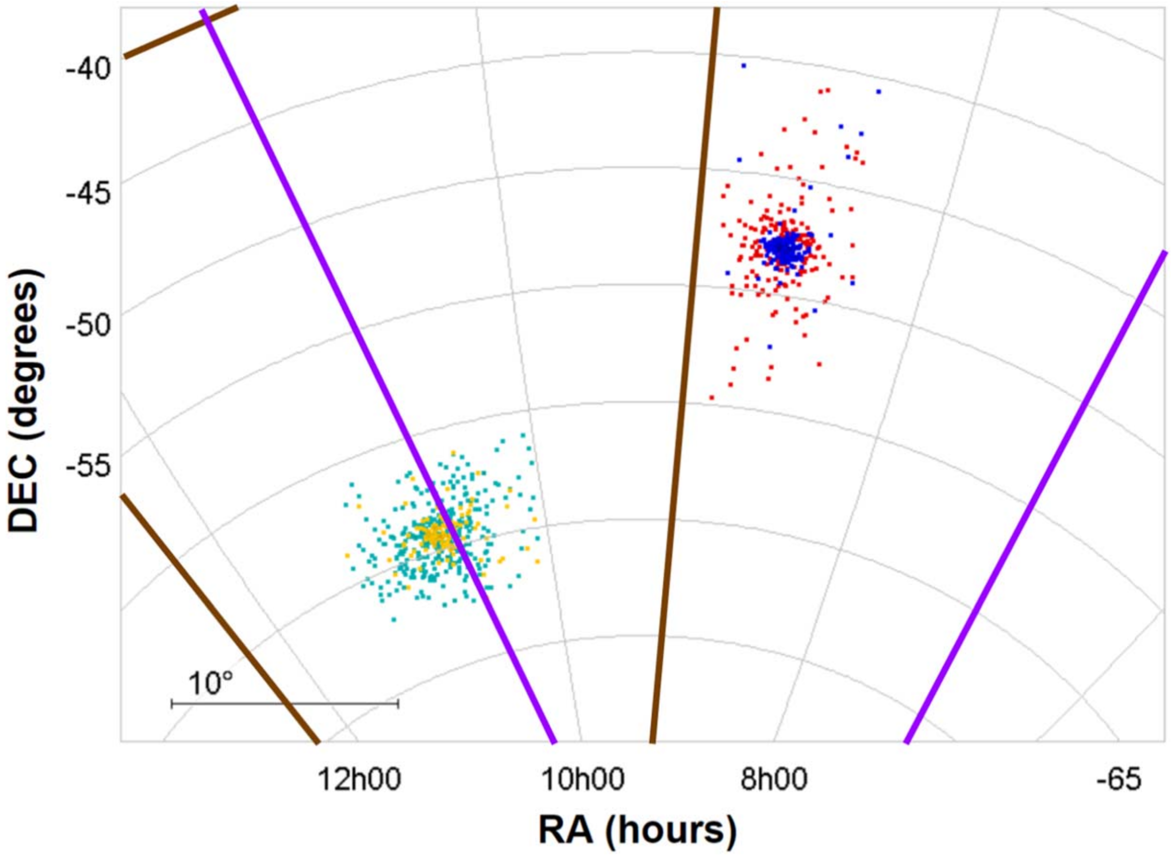

Figure 1. Sky positions for IC 2602 and IC 2391 candidate cluster members identified using the prescription in Section 2. The R.A. and decl. ranges of search regions are shown and extend off the plot (brown for IC 2602 and purple for IC 2391). New and known IC 2391 candidate members are represented by red and blue points, respectively. New and known IC 2602 candidate members are represented by cyan and yellow points, respectively.

In the current work, we utilize the second data release (Gaia DR2; Gaia Collaboration et al. 2018), which provides kinematic and distance information for over one billion stars, to identify potential candidate members of IC 2602 and IC 2391 (Section 2). We obtain high-dispersion optical spectra for all newly identified candidate members of IC 2602 and IC 2391 brighter than $G = 13$ magnitude (Section 3). We use the spectra to measure youth diagnostics, radial and projected rotational velocities, as well as determine stellar properties for each star (Section 3). These measurements allow us to identify new candidate binaries (Section 4), assess cluster membership (Section 5), and characterize ensemble cluster properties (Section 6).

2. Using Gaia DR2 to Identify Candidate Cluster Members

We query the Gaia DR2 archive for candidate cluster members with decl. and R.A. boundaries centered about the average SIMBAD coordinates (Wu et al. 2009) of bona fide members (160°, −65° for IC 2602; 130°, −53° for IC 2391). The boundaries extend 25° in decl. and 1.7 hr in R.A (Figure 1). Within these regions, we identify candidate cluster members using the constraints listed in Table 1 on parallax, proper motion, and measurement uncertainties. We apply a less strict parallax uncertainty constraint for stars brighter than $G = 8$ mag (0.5 versus 0.35 mas), based on the recommendations of Drimmel et al. (2019); brighter stars have parallaxes with larger systematic errors.

Table 1
Properties of Candidate Cluster Members

Cluster	Property	Constraint
IC 2602	R.A. (hr)	$10 \leqslant \text{R.A.} \leqslant 11.3$
	Decl. (deg)	$-67.5 \leqslant \text{Decl.} \leqslant -61$
	ϖ (mas)	$6.2 \leqslant \varpi \leqslant 7.0$
	$\mu_\alpha \cos\delta$ (mas yr^{-1})	$-25 \leqslant \mu_\alpha \cos\delta \leqslant -10$
	μ_δ (mas yr^{-1})	$6 \leqslant \mu_\delta \leqslant 17$
	ϵ_ϖ (mas)	$\epsilon_\varpi \leqslant 0.5$ (if $G \leqslant 8$)
		$\epsilon_\varpi \leqslant 0.35$ (if $G > 8$)
	$\epsilon_{\mu_\alpha \cos\delta}$ (mas yr^{-1})	$\epsilon_{\mu_\alpha \cos\delta} \leqslant 0.8$
	ϵ_{μ_δ} (mas yr^{-1})	$\epsilon_{\mu_\delta} \leqslant 0.8$
IC 2391	R.A. (hr)	$8.3 \leqslant \text{R.A.} \leqslant 9$
	Decl. (deg)	$-60 \leqslant \text{Decl.} \leqslant -45$
	ϖ (mas)	$6.2 \leqslant \varpi \leqslant 7.4$
	$\mu_\alpha \cos\delta$ (mas yr^{-1})	$-31 \leqslant \mu_\alpha \cos\delta \leqslant -19$
	μ_δ (mas yr^{-1})	$15 \leqslant \mu_\delta \leqslant 28$
	ϵ_ϖ (mas)	$\epsilon_\varpi \leqslant 0.5$ (if $G \leqslant 8$)
		$\epsilon_\varpi \leqslant 0.35$ (if $G > 8$)
	$\epsilon_{\mu_\alpha \cos\delta}$ (mas yr^{-1})	$\epsilon_{\mu_\alpha \cos\delta} \leqslant 0.8$
	ϵ_{μ_δ} (mas yr^{-1})	$\epsilon_{\mu_\delta} \leqslant 0.8$

Note. Candidate cluster members are identified based on right-ascension (R.A.), declination (decl.), parallax (ϖ), proper motion in R.A. ($\mu_\alpha \cos\delta$), and proper motion in decl. (μ_δ), as well as uncertainties of parallax (ϵ_ϖ) and proper motion ($\epsilon_{\mu_\alpha \cos\delta, \mu_\delta}$).

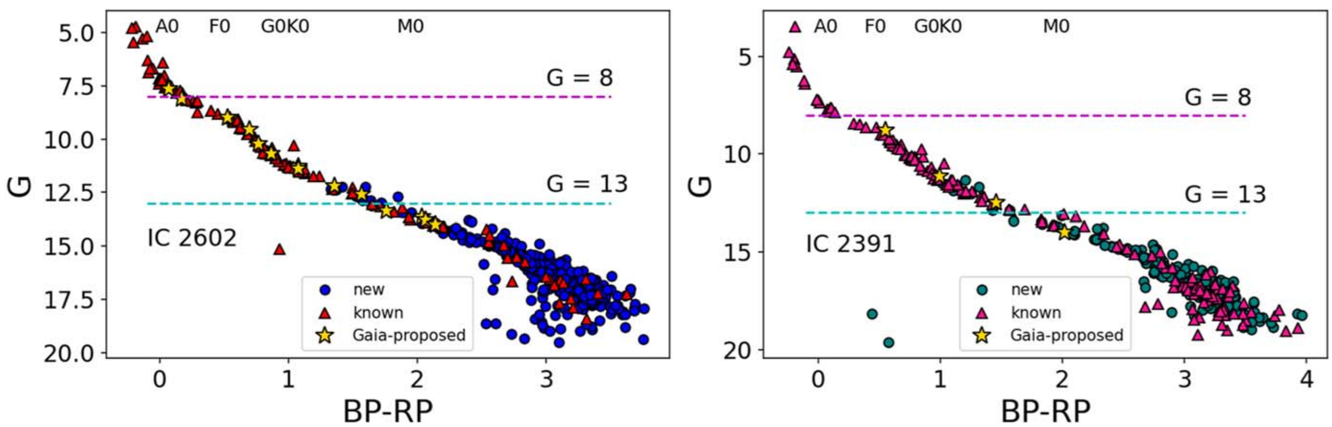

Figure 2. Gaia apparent G magnitude vs. Gaia BP–RP color for 451 candidate members of IC 2602 (left panel) and 350 candidate members of IC 2391 (right panel); the 14 candidate members without Gaia colors (4 in IC 2391 and 10 in IC 2602) are not plotted. For IC 2602, 331 are new (blue circles) while 120 are known (red triangles). For IC 2391, 198 are new (teal circles) while 152 are known (pink triangles). Objects brighter than $G = 14$ in the Gaia DR2 membership lists that are absent from ours are indicated by golden stars. The magenta line shows the brightness ($G = 8$) above which a more lenient parallax constraint is applied in identifying membership (see Section 2). Estimated spectral types are shown at their corresponding Gaia color (Pecaut & Mamajek 2013). We obtain optical spectra for all new candidate members brighter than $G = 13$ (see Section 3).

This prescription identifies 451 candidate members of IC 2602, with G magnitudes spanning from 4.7 to 19.5. Likewise, it identifies 350 candidate members of IC 2391 with G magnitudes spanning from 3.5 to 19.6. These stars are plotted on color–magnitude diagrams in Figure 2.

Considering candidate members with $G < 14$, our membership lists agree with those of the Gaia collaboration (Gaia Collaboration et al. 2018) to 90% (96 stars) and 95% (78 stars) for IC 2602 and IC 2391, respectively. Over the full magnitude range, our prescription yields 46 and 54 candidate members of IC 2602 and IC 2391, respectively, that are not present in the Gaia Collaboration's membership lists. For $G < 14$, we identify 13 and four candidate members of IC 2602 and IC 2391, respectively, which are identified by the Gaia Collaboration, but not by the prescription used in this work. While the single-star main sequences are well-defined for these populations overall, they broaden for $G > 15$ due to larger distance errors; median parallax uncertainties for both clusters are 0.03 mas ($G < 15$), 0.07 mas ($15 < G < 17$), and 0.12 mas ($17 < G$; Gaia Collaboration et al. 2018).

To determine which of our candidate members are known members of these clusters independent of those proposed by the Gaia Collaboration, we conduct a cross-match with SIMBAD (Wenger et al. 2000) through Vizier's X-Match (Ochsenbein et al. 2000) within a $1''$ radius of the Gaia DR2 coordinates. A candidate member is considered to be a known member if (1) the star is present in SIMBAD and (2) the star has been previously classified as a candidate member of the cluster. From this, we determine that our membership lists contain 120 known members and 331 new candidate members for IC 2602, and 152 known members and 198 new candidate members for IC 2391 (see Figures 2 and 3). If these new candidate members are confirmed, the known stellar populations of these clusters will increase by 275% and 130%, respectively.

Renormalized unit weight error (RUWE) values are used in some papers to assess membership of candidate cluster members (Lindegren et al. 2018; Esplin & Luhman 2019; Luhman & Esplin 2020). We do not use RUWE constraints because bright stars and photometric binaries are preferentially excluded. Bright stars are lost because they have large systematic errors in Gaia DR2 astrometry (Drimmel et al. 2019), while photometric binaries are lost because the astrometric χ^2 relies on a single-star model.

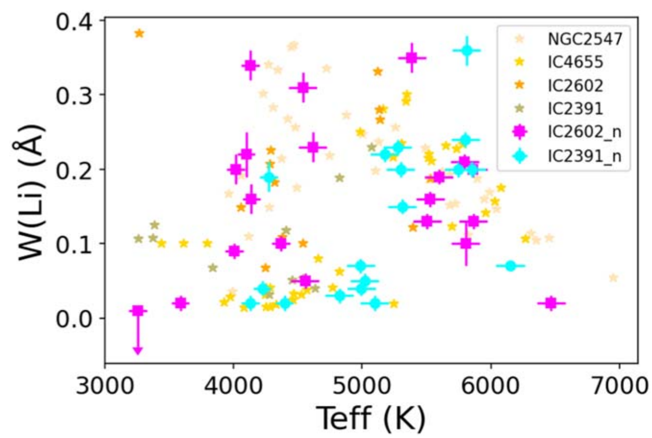

Figure 3. Equivalent widths of lithium at 6708 Å are plotted against effective temperatures (see Section 3.3) for all observed stars in this study for IC 2602 (magenta squares; IC2602_n) and IC 2391 (cyan circles; IC2391_n). Upper limits are indicated with arrows. Here, we show that our lithium measurements for IC 2602 and IC 2391are consistent with those for other clusters of similar age (Gutiérrez Albarrán et al. 2020).

Our new refined membership lists can be found in Appendix Tables A1 (for IC 2391) and A2 (for IC 2602). The lists are sorted by Gaia BP–RP color. For some stars (4 in IC 2391 and 10 in IC 2602), BP–RP color was not provided. Furthermore, the 3 stars with BP–RP < 1 and $G > 13$ are unlikely to be white dwarfs based on their ages. If the Gaia photometry is correct for these, follow-up spectroscopy may confirm them to be background giants (Richer et al. 2021). Because these stars still show similar distance and space motion as per our prescription, we consider them to be candidate members.

3. Spectroscopic Observations and Properties of Candidate Cluster Members

To confirm the membership candidates identified here, we initiate a spectroscopic survey project to acquire high-resolution spectra. We obtain spectra for all 26 bright ($G < 13$) candidate members newly identified in this study to confirm cluster membership. We also observe 12 previously

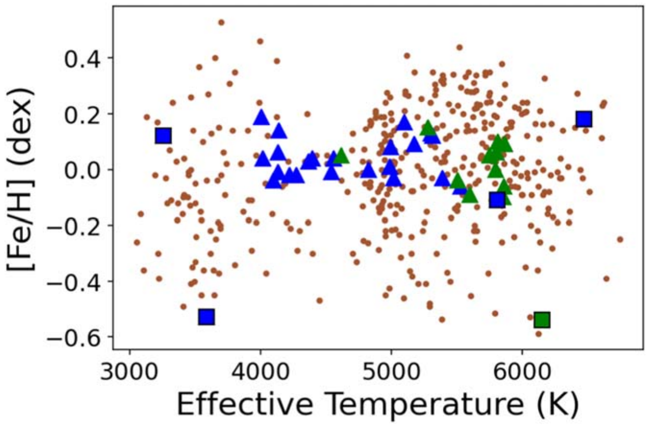

Figure 4. Metallicity is plotted against effective temperature for the 393 spectral standards (dwarf stars with $3 < \log(g) < 5$) used in the Empirical SpecMatch spectral library (red points). Previously known members and new candidate members observed in this study are colored green and blue, respectively. Stars are marked as squares if they are candidate double-lined spectroscopic binaries (see Section 4.2) and triangles if they are not.

known (also with $G < 13$) cluster members to check the reliability of our analysis techniques. We obtain single-epoch 1200 s exposures for each star using the CHIRON echelle spectrograph (Tokovinin et al. 2013; Paredes et al. 2021) on the CTIO/SMARTS 1.5 m telescope. The stars are observed in fiber mode, which covers 4500–8900 Å over 62 spectral orders at a resolving power of $R \sim 27{,}400$. We also obtain a thorium-argon lamp spectrum before each object spectrum for wavelength calibration. The RECONS team at Georgia State University process the observed echelle spectra from CHIRON to provide wavelength-calibrated spectral orders, as described in Tokovinin et al. (2013). In order to measure radial and projected rotational velocities, single-epoch spectra of CHIRON standards[1] (A. Yep et al. 2022, in preparation) are also obtained using the same spectral setup.

3.1. Li I λ6708 Å and Hα Equivalent Widths

As a first assessment of stellar youth, we measure equivalent widths of the lithium doublet at 6708 Å and the Hα feature at 6563 Å using IRAF's Gaussian-fitting *splot* package. We estimate equivalent width uncertainties using the spectrograph pixel-wavelength scale p (0.097 Å at Hα; 0.100 Å at lithium), the measured Gaussian full width at half maximum f of the spectral line, and the signal-to-noise ratio per pixel, following the prescription of Cayrel (1988) and Deliyannis et al. (1993, 2019):

$$\Delta \mathrm{EW} \simeq 1.5 \frac{\sqrt{fp}}{S/N}. \tag{1}$$

When reporting equivalent widths, we adopt the standard convention of assigning negative values for emission lines and positive values for absorption. Upper limits are assigned when the spectral line cannot be distinguished from the noise of the continuum. For the candidate double-lined spectroscopic binaries (see Section 4.2), equivalent widths are diminished due to the companion's continuum. The measured equivalent widths of lithium absorption are plotted as a function of effective temperature in Figure 3. The distributions of values are consistent with measurements in clusters with similar age

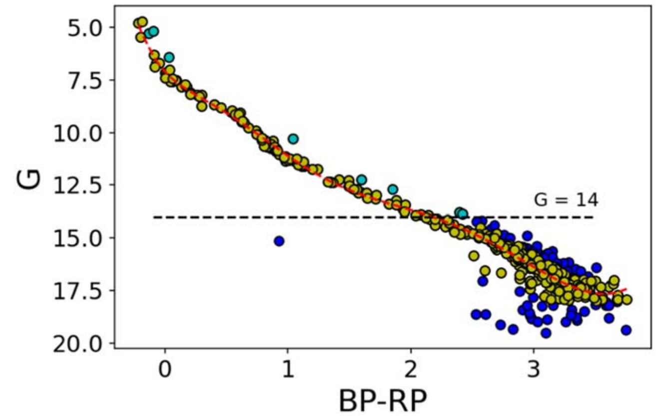

Figure 5. Candidate photometric binaries are identified in IC 2602 by an iterative fit to the main sequence (down to $G < 18$). Stars retained in the fit are shown as yellow circles. For stars brighter than $G = 14$, any star more than 0.6 mag above the fit are considered candidate binaries (cyan circles). For stars fainter than $G = 14$ (blue circles), we do not identify binaries because of the broader main sequence.

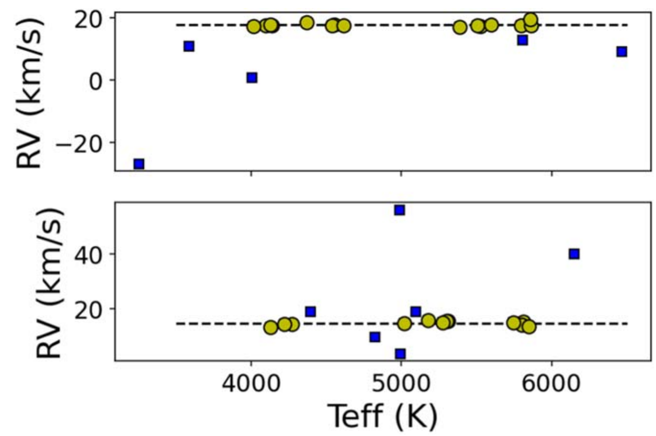

Figure 6. Distribution of RVs for spectroscopically observed stars in IC 2602 (top panel) and IC 2391 (bottom panel) as a function of effective temperature. Candidate binary stars (blue squares) are identified by iterative fits to the mean RVs (dotted black lines) of the ensembles; yellow circles are not candidate binaries.

(30–50 Myr based on their main-sequence turnoffs) from Gutiérrez Albarrán et al. (2020). Compared with literature values in previously known members (as reported by Randich et al. 1997, 2001; Platais et al. 2007), our measured values agree within measurement uncertainties (∼0.02 Å). Equivalent width values are listed in Tables 3 and 4. New candidate members are designated with the internal identifiers ALN if they are in IC 2602 and NTC if they are in IC 2391.

3.2. Radial and Rotational Velocities

To measure the radial velocities (RVs) and projected rotational velocities ($v \sin i$) of target stars, we perform normalized cross-correlation of 12 spectral orders (4990–6860 Å). We avoid those with telluric absorption (e.g., A-band, B-band), chromospheric emission (e.g., Hα), and pressure-sensitive lines that may bias the $v \sin i$ results, between the target and three spectral standards of similar Gaia BP–RP color.

[1] https://github.com/alexandrayep/CHIRON_Standards

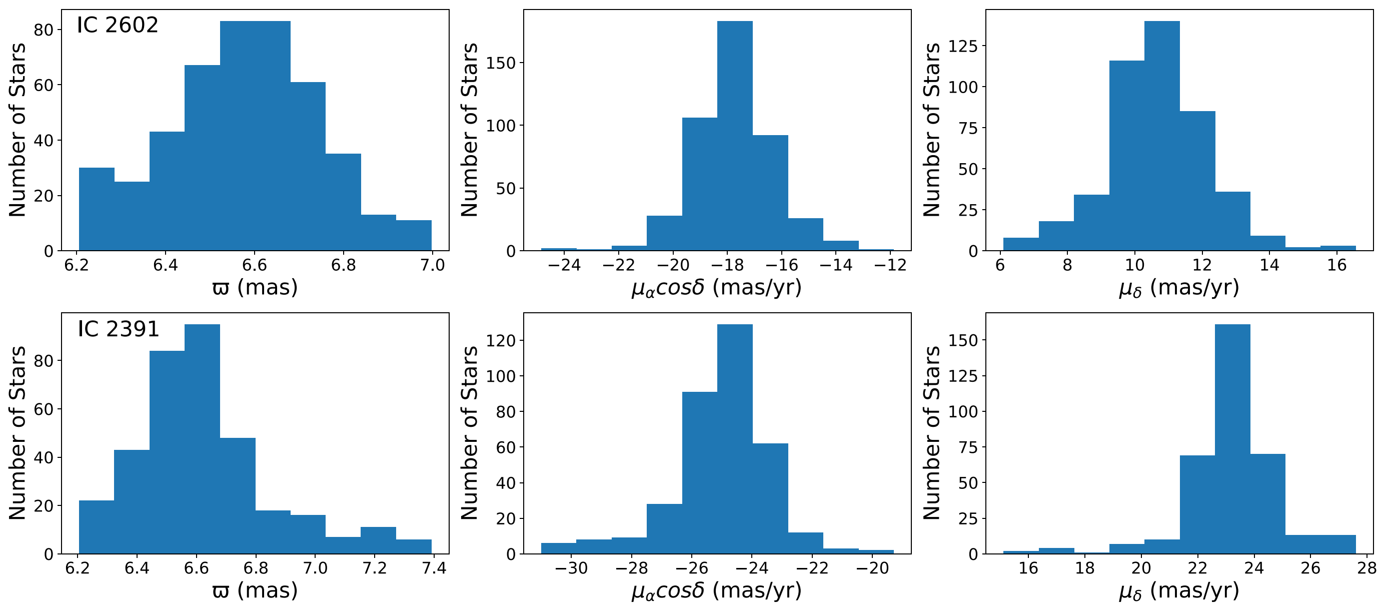

Figure 7. For all 451 members of IC 2602 (top panels) and all 350 members of IC 2391 (bottom panels), histograms of parallax (left panels), proper motion in R.A. (center panels), and proper motion in decl. (right panels) are shown. Ensemble values for the distributions of these properties are listed in Table 2.

A radial velocity is determined from each spectral order by fitting the peak of the cross-correlation function (CCF) with a Gaussian. The radial-velocity uncertainty for each spectral order is estimated using the equation from Butler et al. (1996). By weighing these relative radial velocities by their corresponding Doppler uncertainties, a weighted mean relative radial velocity is calculated. Barycentric velocities are determined using EXOFAST's (Eastman et al. 2013) barycentric correction algorithm (Wright & Eastman 2014) and PyAstronomy's *helcorr* function.

We determine projected rotational velocities by creating an empirical relation between the CCF width and $v \sin i$, by cross-correlating each standard star spectrum against rotationally broadened synthetic versions of itself (using PyAstronomy's *rotBroad* function; Gray 1976, 1992; White et al. 2007). To obtain our final $v \sin i$ estimates, we average the $v \sin i$ measurements for all orders, taking the standard deviation of these as the uncertainty, and then calculate the weighted average of resulting $v \sin i$ estimates provided by three standard stars. We find that our measured radial and projected rotational velocities agree within two standard deviations of published literature values. Values are listed in Table 4.

3.3. Stellar Fundamental Parameters

We measure the stellar properties of the 38 observed stars using Empirical SpecMatch (Yee et al. 2017). This Python code determines stellar parameters of a spectrum by comparing it to a dense library of spectral standards. The code employs nonlinear least-squares minimization (Newville et al. 2014) to minimize χ^2 when (1) obtaining the best-matching library spectra, allowing continuum normalization and $v \sin i$ provided by the SpecMatch program to float as free parameters, and (2) generating the best-matching linear combination of library spectra to determine stellar properties.

Figure 4 illustrates the best-fit metallicities versus effective temperatures of candidate cluster members, along with the values of the comparison standards from which these values were determined. Stellar properties for the candidate double-lined spectroscopic binaries (including the two stars with [Fe/H] < -0.5) marked in Tables 3 and 4 are unreliable due to contamination of spectra by companions.

Using previously known members to test Empirical SpecMatch, we find that our derived properties for single-star members are consistent to within the uncertainties of published literature values (Marsden et al. 2009; De Silva et al. 2013; Randich et al. 2018). Best-fit effective temperatures, surface gravities, and metallicities for new and know members are listed in Tables 3 and 4, respectively.

4. New and Candidate Binaries

We find new candidate photometric and spectroscopic binaries based on the following analyses.

4.1. New Candidate Photometric Binaries

Unresolved multiple star systems with companions of comparable brightness are expected to be positioned above the single-star main sequence (Cantat-Gaudin et al. 2018). To identify candidate photometric binaries, we use eighth-order polynomials to iteratively fit the main sequences for stars brighter than $G = 18$ magnitude of these clusters. We classify candidate binary stars as those that sit above the fit by at least 0.6 mag (see Figure 5); this is roughly 0.2 standard deviations above the best-fit main sequences. While we can be confident this prescription works down to $G \sim 14$, the prescription fails at dimmer magnitudes due to the spread in the main sequence. Considering only candidate members with $G < 14$, we identify 18 candidate photometric binaries. We find that 14 of these are previously known cluster members (seven in IC 2602 and seven in IC 2391) while four are new (two in IC 2602 and two in IC 2391). Candidate photometric binaries are marked in Tables 3 and 4.

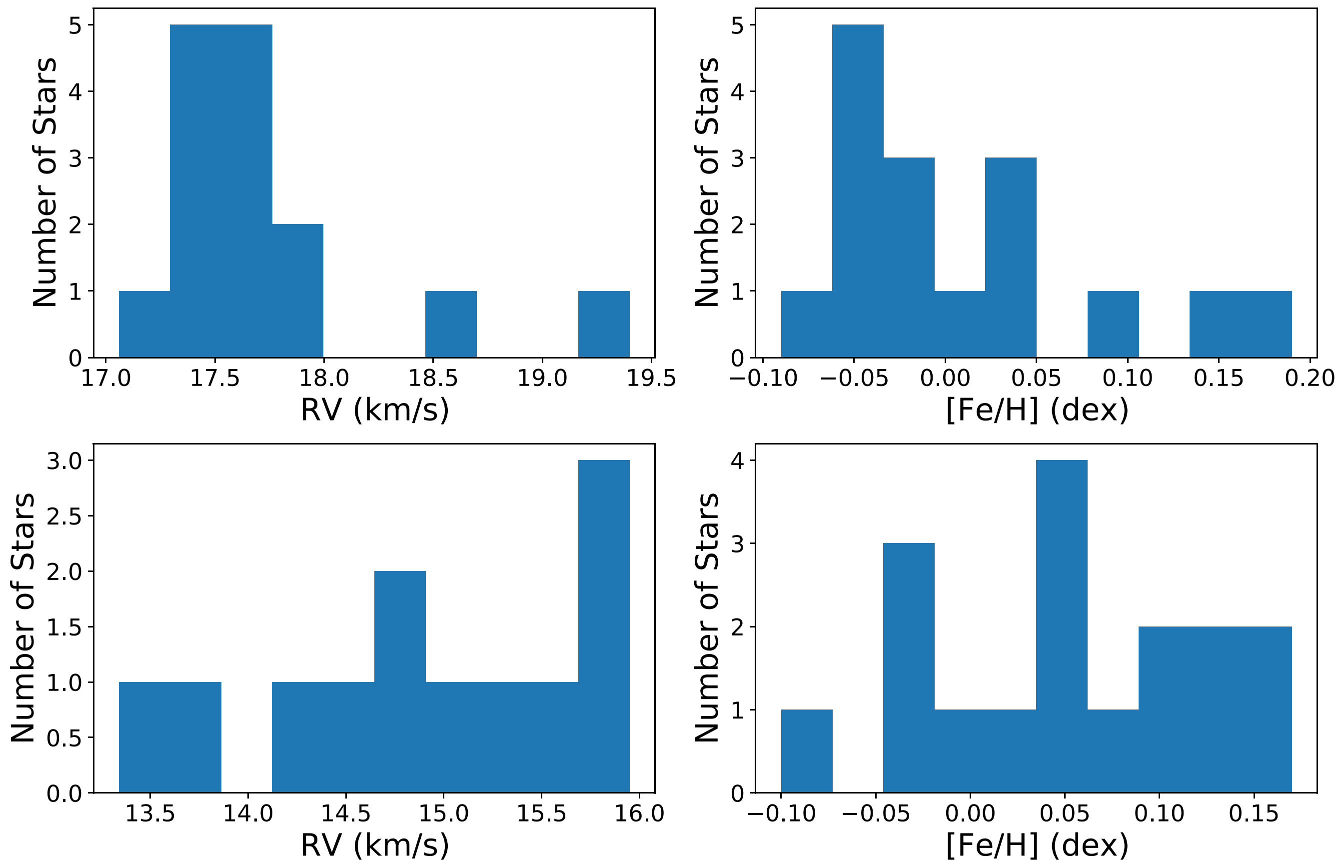

Figure 8. Histograms of radial velocity (left panels) and metallicity (right panels) for IC 2602 (top panels) and IC 2391 (bottom panels) are shown. Binaries are excluded as described in Section 6. Ensemble values for the distributions of these properties are listed in Table 2.

4.2. New Candidate Spectroscopic Binaries

Cluster members with RVs significantly different from the mean RVs of cluster stars may be spectroscopic binaries (Platais et al. 2007). To identify such candidate spectroscopic binaries, we iteratively fit the mean RVs of cluster stars within 3 standard deviations. To obtain the best fit (see Figure 6), we regard as candidate spectroscopic binaries those stars with RVs different from the resulting means of the ensembles by more than 3 km s^{-1} ($\sim$1 standard deviation). Given that the internal radial-velocity dispersions of these clusters is expected to be less than 1 km s^{-1} (Stauffer et al. 1997), we have applied a more stringent constraint for our 43-52 Myr clusters than the prescription used by Hayes & Friel (2014) for 1–3 Gyr clusters (3 km s^{-1} versus 5 km s^{-1}). The stars we do not flag as candidate spectroscopic binaries are used to estimate the cluster's radial velocities and dispersions in Section 6.

Of the 11 new candidate spectroscopic binaries we identify (five in IC 2602, six in IC 2391), we find that five are double-lined (four in IC 2602, one in IC 2391) and six are single-lined (one in IC 2602, five in IC 2391). These binaries are marked in Tables 3 and 4.

5. Confirmation of New Candidate Members

We use the presence of lithium absorption or Hα emission to assign membership for candidate members. We observe that 19 of 20 IC 2602 stars show lithium absorption while 12 of 20 show Hα emission; 11 stars show both. Furthermore, we observe that

Table 2
Summary of Ensemble Cluster Properties

Property	Value	Std. Dev.
IC 2602		
Center R.A. (deg)	160.524 ± 0.004	$3.585(52\sigma_{mn})$
Center Decl. (deg)	-64.387 ± 0.004	$1.231(18\sigma_{mn})$
Avg.ϖ (mas)	6.576 ± 0.004	$0.170(2.2\sigma_{mn})$
Avg. $\mu_\alpha \cos\delta$ (mas yr^{-1})	-17.740 ± 0.009	$1.528(11\sigma_{mn})$
Avg. μ_δ (mas yr^{-1})	10.669 ± 0.008	$1.530(12\sigma_{mn})$
Avg. Distance (pc)	$151.58^{+1.87}_{-1.80}$	$3.90(2.1\sigma_{mn})$
Age (Myr)	$43.7^{+4.3}_{-3.9}$ (B18)	
Avg. RV (km s^{-1})	17.73 ± 0.04	$0.56(3.9\sigma_{mn})$
Avg. [Fe/H] (dex)	0.02 ± 0.02	$0.07(0.8\sigma_{mn})$
IC 2391		
Center R.A. (deg)	130.276 ± 0.005	$1.630(24\sigma_{mn})$
Center Decl. (deg)	-52.923 ± 0.005	$1.763(23\sigma_{mn})$
Avg.ϖ (mas)	6.628 ± 0.005	$0.228(2.9\sigma_{mn})$
Avg. $\mu_\alpha \cos\delta$ (mas yr^{-1})	-25.005 ± 0.010	$1.590(10\sigma_{mn})$
Avg. μ_δ (mas yr^{-1})	23.236 ± 0.011	$1.609(10\sigma_{mn})$
Avg. Distance (pc)	$150.44^{+1.86}_{-1.79}$	$4.99(2.7\sigma_{mn})$
Age (Myr)	$51.3^{+5.0}_{-4.5}$ (B18)	
Avg. RV (km s^{-1})	14.88 ± 0.04	$0.78(5.6\sigma_{mn})$
Avg. [Fe/H] (dex)	0.05 ± 0.02	$0.07(0.8\sigma_{mn})$

Note. Ensemble cluster property values and uncertainties are listed in Column 2 while standard deviations are compared with mean individual uncertainties (σ_{mn}) in Column 3. Here, the reference B18 refers to Bravi et al. (2018).

Table 3
Measurements for 26 New Candidate Members of IC 2602 and IC 2391

Identifier		Measurements from CHIRON Spectra				Stellar Parameters from SpecMatch		
Internal	2MASS	RV (km s^{-1})	$v \sin i$ (km s^{-1})	EW[Li] (Å)	EW[Hα] (Å)	$T_{\rm eff}$ (K)	log(g) (dex)	[Fe/H] (dex)
IC 2602								
ALN 1	10420316-6520590	17.37 ± 0.12	7.6 ± 0.8	0.16 ± 0.01	0.76 ± 0.02	5527 ± 110	4.53 ± 0.12	-0.06 ± 0.09
ALN 2	10414173-6222205	17.06 ± 0.19	23.4 ± 2.2	0.35 ± 0.02	0.02 ± 0.01	5385 ± 110	4.50 ± 0.12	-0.03 ± 0.09
ALN 3[iii]	10411756-6526576	-26.69 ± 0.20	17.4 ± 5.6	$<0.01 \pm 0.01$	-0.02 ± 0.01	3257 ± 70	4.86 ± 0.12	0.12 ± 0.09
ALN 4	10384893-6330430	17.69 ± 0.12	4.6 ± 1.8	0.05 ± 0.01	0.72 ± 0.03	4556 ± 110	4.60 ± 0.12	0.04 ± 0.09
ALN 5[i,iii]	10385502-6257272	10.88 ± 0.21	19.6 ± 6.4	0.02 ± 0.01	-0.24 ± 0.02	3586 ± 70	4.83 ± 0.12	-0.53 ± 0.09
ALN 6[iii]	10591218-6438089	9.28 ± 0.21	23.3 ± 6.6	0.02 ± 0.01	-0.11 ± 0.01	6465 ± 110	3.86 ± 0.12	0.18 ± 0.09
ALN 7	10322955-6506403	17.47 ± 0.17	13.6 ± 1.3	0.31 ± 0.02	-0.03 ± 0.01	4537 ± 110	4.61 ± 0.12	-0.01 ± 0.09
ALN 8	10482786-6554502	17.44 ± 0.16	9.2 ± 1.8	0.22 ± 0.03	-0.26 ± 0.02	4098 ± 70	4.68 ± 0.12	-0.04 ± 0.09
ALN 9	10200052-6217465	18.61 ± 0.15	7.7 ± 1.6	0.10 ± 0.01	-0.25 ± 0.02	4367 ± 70	4.65 ± 0.12	0.03 ± 0.09
ALN 10[ii]	10280304-6316132	0.68 ± 0.18	26.0 ± 4.2	0.09 ± 0.01	-0.63 ± 0.02	4006 ± 70	4.67 ± 0.12	0.19 ± 0.09
ALN 11	10521914-6558069	17.55 ± 0.15	7.4 ± 1.5	0.16 ± 0.02	-0.70 ± 0.02	4138 ± 70	4.66 ± 0.12	0.14 ± 0.09
ALN 12[i,iii]	10521708-6502488	12.78 ± 0.13	20.0 ± 5.6	0.10 ± 0.03	-1.30 ± 0.05	5804 ± 110	4.28 ± 0.12	-0.11 ± 0.09
ALN 13	10353048-6218367	17.40 ± 0.16	8.2 ± 1.8	0.20 ± 0.02	-0.85 ± 0.02	4017 ± 70	4.69 ± 0.12	0.04 ± 0.09
ALN 14	10315315-6234333	17.79 ± 0.17	13.0 ± 1.3	0.34 ± 0.02	-0.66 ± 0.02	4131 ± 70	4.67 ± 0.12	-0.01 ± 0.09
IC 2391								
NTC 1	08202510-5340306	15.95 ± 0.12	4.6 ± 2.0	0.22 ± 0.01	-0.22 ± 0.02	5175 ± 110	4.51 ± 0.12	0.09 ± 0.09
NTC 2	08320021-5539048	14.43 ± 0.16	9.5 ± 1.0	0.19 ± 0.02	-0.41 ± 0.02	4272 ± 70	4.66 ± 0.12	-0.02 ± 0.09
NTC 3[ii]	08365944-5219251	19.08 ± 0.14	7.0 ± 1.6	0.02 ± 0.01	0.55 ± 0.03	4395 ± 70	4.64 ± 0.12	0.04 ± 0.09
NTC 4	08372464-5254109	14.67 ± 0.16	7.9 ± 1.2	0.04 ± 0.01	-0.54 ± 0.02	4222 ± 70	4.66 ± 0.12	-0.02 ± 0.09
NTC 5	08383609-5206388	13.34 ± 0.21	27.2 ± 3.9	0.02 ± 0.01	-0.23 ± 0.01	4131 ± 70	4.67 ± 0.12	0.06 ± 0.09
NTC 6	08433845-5130289	15.76 ± 0.11	7.2 ± 0.7	0.15 ± 0.01	0.72 ± 0.02	5310 ± 110	4.48 ± 0.12	0.12 ± 0.09
NTC 7	08433893-5130249	15.73 ± 0.11	5.8 ± 2.3	0.20 ± 0.01	0.67 ± 0.02	5298 ± 110	4.47 ± 0.12	0.13 ± 0.09
NTC 8[ii]	08443450-5255325	18.88 ± 0.09	5.1 ± 1.4	0.02 ± 0.01	0.82 ± 0.02	5097 ± 110	4.54 ± 0.12	0.17 ± 0.09
NTC 9[i,ii]	08473860-5216099	9.80 ± 0.13	9.3 ± 1.0	0.03 ± 0.01	0.33 ± 0.01	4823 ± 110	4.46 ± 0.12	0.00 ± 0.09
NTC 10[ii]	08583097-5040359	3.77 ± 0.11	7.0 ± 1.0	0.04 ± 0.01	0.76 ± 0.02	4993 ± 110	4.52 ± 0.12	0.08 ± 0.09
NTC 11[i]	08583180-5040360	14.81 ± 0.11	8.3 ± 1.3	0.05 ± 0.01	0.77 ± 0.02	5018 ± 110	4.55 ± 0.12	-0.03 ± 0.09
NTC 12[ii]	08593213-5106511	55.92 ± 0.12	4.6 ± 1.9	0.07 ± 0.01	0.93 ± 0.02	4987 ± 110	4.53 ± 0.12	0.01 ± 0.09

Notes. New candidate binaries are indicated as.
[i] Photometric.
[ii] Single-lined spectroscopic.
[iii] Double-lined spectroscopic. Stars flagged as candidate double-lined spectroscopic binaries have biased equivalent widths and SpecMatch properties so those measurements are suspect in the table.

all 18 IC 2391 stars show lithium absorption while five of 18 show Hα emission.

The double-lined spectroscopic binary, ALN 3, is the star without detectable lithium absorption noted above. While ALN 3 shows Hα emission, a known youth indicator in pre-main-sequence stars (Barrado et al. 2000; Casey et al. 2016; Gutiérrez Albarrán et al. 2020), such emission can also be produced by close-interacting field binaries (Vesper & Honeycutt 1993; Wevers et al. 2016). Since it is still possible that ALN 3 has weak lithium absorption diluted by the flux of a companion, we regard the membership of ALN 3 to IC 2602 to be uncertain.

Based on consistent distances, sky positions, proper motions, and the presence of lithium absorption or Hα emission, we conclude that 19 of 20 IC 2602 and 18 IC 2391 candidate members are bona fide cluster members. In combination with previously known members, 133 (29%) of IC 2602 and 164 (47%) of IC 2391are spectroscopically confirmed members. Measurements are listed and binarity is indicated for these stars in Tables 3 and 4.

6. Ensemble Cluster Properties

We use the newly assembled measurements to determine ensemble cluster properties for IC 2602 and IC 2391. Using kinematic candidate members we identify in Section 2 (451 stars in IC 2602, 350 stars in IC 2391), we estimate new mean right ascensions, declinations, parallaxes, and proper motions for cluster stars. The distributions for these astrometric properties are illustrated in Figure 7. We compute mean distances using the values calculated by Bailer-Jones et al. (2018). For completeness, we list cluster ages from Bravi et al.(2018).

For spectroscopically determined properties, candidate spectroscopic binaries are excluded from the average cluster RVs and double-lined binaries are excluded from the average metallicities (see Section 4.2). In total, 15 IC 2602 and 12 IC 2391 stars are used to estimate mean RVs while 16 IC 2602 and 17 IC 2391 stars are used to estimate mean metallicities. The distribution of spectroscopic properties for these stars are illustrated in Figure 8. Our measured ensemble values agree with literature values to within the uncertainties of previous estimates (as reported by Randich et al. 2001; Platais et al. 2007; Marsden et al. 2009).

IC 2602 has central positions at R.A. $= 160.524 \pm 0.004$ and decl. $= -64^\circ\!.387 \pm 0^\circ\!.004$ where errors represent uncertainties in the means. IC 2602 members have an average distance of 151.58 pc, with an uncertainty in the mean of $\sim$1.8 pc and a standard deviation of 3.90 pc that is 2.1 times larger than the average distance uncertainty. IC 2602 members have a mean RV

Table 4
Measurements for 12 Known Members of IC 2602 and IC 2391

Name	Measurements from CHIRON Spectra						Stellar Parameters from SpecMatch			
	RV (km s^{-1})	RV Lit. (km s^{-1})	$v \sin i$ (km s^{-1})	$v \sin i$ Lit. (km s^{-1})	EW[Li] (Å)	EW[Hα] (Å)	$T_{\rm eff}$ (K)	$T_{\rm eff}$ Lit. (K)	log(g) (dex)	[Fe/H] (dex)
IC 2602										
W79	17.53 ± 0.11	17.4(R18)	7.8 ± 1.0	8(M09)	0.13 ± 0.01	0.83 ± 0.02	5505 ± 110	5500(M09)	4.52 ± 0.12	−0.04 ± 0.09
R1	17.90 ± 0.11	18(M09)	8.4 ± 0.9	<10(R01)	0.19 ± 0.01	0.60 ± 0.02	5596 ± 110	5320(M09)	4.53 ± 0.12	−0.09 ± 0.09
R10	17.61 ± 0.16	19(M09)	14.9 ± 1.2	14(M09)	0.23 ± 0.02	−0.08 ± 0.01	4614 ± 110	4520(M09)	4.60 ± 0.12	0.05 ± 0.09
R66	17.64 ± 0.13	17.4(R18)	12.0 ± 0.9	12(S97)	0.21 ± 0.01	0.62 ± 0.02	5795 ± 110	5792(R18)	4.47 ± 0.12	0.00 ± 0.09
R70	17.43 ± 0.11	17.4(R18)	10.8 ± 1.1	11(S97)	0.13 ± 0.01	0.88 ± 0.01	5862 ± 110	5854(R18)	4.51 ± 0.12	0.09 ± 0.09
SR3	19.40 ± 0.13	15.3(Me09)	13.2 ± 1.2	14.7(Me09)	0.20 ± 0.01	0.89 ± 0.01	5860 ± 110	N/A	4.41 ± 0.12	−0.06 ± 0.09
IC 2391										
VXR16A	15.49 ± 0.19	15.5(S97)	20.8 ± 1.9	20.7(Me09)	0.36 ± 0.02	−0.12 ± 0.01	5810 ± 110	5130(M09)	4.51 ± 0.12	0.10 ± 0.09
VXR22A	14.26 ± 0.11	14.0(D13)	8.4 ± 0.6	8(M09)	0.24 ± 0.01	0.35 ± 0.01	5800 ± 110	5700(D13)	4.52 ± 0.12	0.06 ± 0.09
VXR70	13.83 ± 0.16	13.8(D13)	15.9 ± 0.8	16(M09)	0.20 ± 0.01	0.59 ± 0.02	5850 ± 110	5819(R18)	4.42 ± 0.12	−0.10 ± 0.09
PMM4362	15.14 ± 0.10	15.11(Pl07)	9.2 ± 0.6	9.0(Me09)	0.20 ± 0.01	0.91 ± 0.01	5746 ± 110	5740(M09)	4.52 ± 0.12	0.05 ± 0.09
SHJM6	15.20 ± 0.13	15.2(D13)	10.9 ± 0.8	10(M09)	0.23 ± 0.01	0.33 ± 0.01	5276 ± 110	5210(M09)	4.48 ± 0.12	0.15 ± 0.09
L37[i,iii]	39.81 ± 0.13	31.69(Me09)	11.0 ± 1.4	11.8(Me09)	0.07 ± 0.00	0.64 ± 0.01	6150 ± 110	5900(M09)	4.09 ± 0.12	−0.54 ± 0.09

Notes. Known binaries are indicated as:
[i] Photometric.
[ii] Single-lined spectroscopic.
[iii] Double-lined spectroscopic. Stars flagged as known double-lined spectroscopic binaries have biased equivalent widths and SpecMatch properties so those measurements are suspect in the table. The references are as follows: D13 = De Silva et al. (2013), M09 = Marsden et al. (2009) Me09 = Mermilliod et al. (2009), Pl07 = Platais et al. (2007), R01 = Randich et al. (2001), R18 = Randich et al. (2018), S97 = Stauffer et al. (1997).

of 17.73 km s^{-1} with an uncertainty in the mean of 0.04 km s^{-1} and a standard deviation of 0.56 km s^{-1} that is 3.9 times larger than the average RV uncertainty.

IC 2391 has central positions at R.A. = 130.276 ± 0.005 and decl. = −52°.923 ± 0°.005 where errors represent uncertainties in the means. IC 2391 members have an average distance of 150.44 pc, with an uncertainty in the mean of ∼1.8 pc and a standard deviation of 4.99 pc that is 2.7 times larger than the average distance uncertainty. IC 2391 members have a mean RV of 14.88 km s^{-1} with an uncertainty in the mean of 0.04 km s^{-1} and a standard deviation of 0.78 km s^{-1} that is 5.6 times larger than the average RV uncertainty.

Given that the standard deviation of RVs is ∼0.8 km s^{-1} in IC 2391 and ∼0.6 km s^{-1} in IC 2602, we confirm that the standard deviations in these clusters is <1 km s^{-1} (Stauffer et al. 1997) and our results are in keeping with the claim that older clusters have larger RV dispersions (Hayes & Friel 2014). For the cluster properties we measure (with the exception of metallicity), standard deviations are larger than both ensemble and mean individual uncertainties. This implies that the observed spread in cluster properties is real and not an artifact of measurement errors. Values are assembled in Table 2.

7. Summary

We use Gaia DR2 positions, space motions, and photometry to map out the stellar populations of IC 2602 and IC 2391. Using CHIRON spectra and Empirical SpecMatch, we determine stellar properties and measure signatures of youth for 38 stars. On the basis of this analysis, we obtain the following main results:

1. We refine the single-star main sequences of IC 2602 (451 stars) and IC 2391 (350 stars). We find a large population of new candidate cluster members (331 stars in IC 2602, 198 stars in IC 2391), never reported before in the literature. The refined membership lists are useful for calibrating models of stellar evolution, planet formation, and migration.
2. We identify new candidate photometric (four stars) and spectroscopic (10 stars) binaries; six of the latter are single-lined while four are double-lined. These findings can be used to improve binary fraction estimates in these clusters. If follow-up observations reveal them to be eclipsing binaries as well, the data can be used to improve stellar evolution models and relations.
3. We determine radial and projected rotational velocities, equivalent widths of lithium and Hα, effective temperatures, surface gravities, and metallicities for all 38 stars observed. We confirm that 13 IC 2602 and 12 IC 2391 new candidate members are bona fide cluster members. This increases the known stellar populations of these clusters (120 stars in IC 2602; 152 stars in IC 2391) by 12% and 8%, respectively.
4. The data enable new, more precise ensemble stellar properties (Table 2).

We are indebted to members of the SMARTS Consortium and NSF's National Optical-Infrared Astronomy Research Laboratory, especially the staff at CTIO, for efforts to keep the SMARTS/CTIO 1.5 m telescope and CHIRON spectrograph in operation. This research has used data from the CTIO/SMARTS 1.5 m telescope, which is operated as part of the SMARTS Consortium by RECONS (www.recons.org) members Todd Henry, Hodari James, Wei-Chun Jao, Leonardo Paredes, and Azmain Nisak. At the telescope, observations were carried out by Roberto Aviles and Rodrigo Hinojosa. This research has made use of the SIMBAD database, operated at CDS, Strasbourg, France. This research has made use of the VizieR catalog access tool, CDS, Strasbourg, France (doi:10.26093/cds/vizier). The original description of the VizieR service was published in 2000, A&AS 143, 23.

Appendix

The refined membership lists for IC 2391 and IC 2602 are tabulated below (see Tables A1 and A2) according to the prescriptions in Section 2. The full tables are available online.

Table A1
Refined Membership List of IC 2391

2MASS	R.A. (h:m:s)	Decl. (d:m:s)	ϖ (mas)	ϵ_{ϖ} (mas)	$\mu_{\alpha}\cos\delta$ (mas yr^{-1})	$\epsilon_{\mu_{\alpha}\cos\delta}$ (mas yr^{-1})	μ_{δ} (mas yr^{-1})	$\epsilon_{\mu_{\delta}}$ (mas yr^{-1})	G (mag)	BP–RP (mag)
08422538-5306501	08:42:25.34	−53:06:49.97	7.11	0.23	−24.58	0.38	22.77	0.46	4.78	−0.24
08392384-5326230	08:39:23.80	−53:26:22.80	6.53	0.14	−25.79	0.31	21.19	0.32	5.42	−0.21
08395759-5303170	08:39:57.55	−53:03:16.65	6.76	0.21	−25.43	0.39	22.32	0.40	5.14	−0.20
08401759-5255190	08:40:17.54	−52:55:18.54	6.59	0.41	−30.56	0.78	21.43	0.76	3.47	−0.19
08401745-5300554	08:40:17.42	−53:00:55.07	6.46	0.09	−24.79	0.17	23.08	0.16	5.52	−0.18

Note. Example data for IC 2391 candidate cluster members identified using the prescription in Section 2. The complete table of 350 candidate members is provided online. Here, the astrometric and photometric parameter values are concatenated to two decimal places.

(This table is available in its entirety in machine-readable form.)

Table A2
Refined Membership List of IC 2602

2MASS	R.A. (h:m:s)	Decl. (d:m:s)	ϖ (mas)	ϵ_{ϖ} (mas)	$\mu_{\alpha}\cos\delta$ (mas yr^{-1})	$\epsilon_{\mu_{\alpha}\cos\delta}$ (mas yr^{-1})	μ_{δ} (mas yr^{-1})	$\epsilon_{\mu_{\delta}}$ (mas yr^{-1})	G (mag)	BP–RP (mag)
10465124-6423005	10:46:51.18	−64:23:00.35	6.34	0.19	−18.92	0.33	9.45	0.30	4.78	−0.22
10401142-6506006	10:40:11.40	−65:06:00.59	6.49	0.12	−19.31	0.20	9.56	0.19	5.45	−0.20
10440694-6357400	10:44:06.87	−63:57:39.71	6.81	0.46	−15.03	0.45	11.41	0.56	4.72	−0.19
10461656-6430526	10:46:16.51	−64:30:52.25	6.41	0.11	−16.19	0.20	10.85	0.18	5.28	−0.13
10462961-6415475	10:46:29.55	−64:15:47.51	6.76	0.17	−17.9	0.29	9.54	0.27	5.17	−0.10

Note. Example data for IC 2602 candidate cluster members identified using the prescription in Section 2. The complete table of 451 candidate members is provided online. Here, the astrometric and photometric parameter values are concatenated to two decimal places.

(This table is available in its entirety in machine-readable form.)

ORCID iDs

Azmain H. Nisak https://orcid.org/0000-0002-1457-1467
Russel J. White https://orcid.org/0000-0001-5313-7498
Alexandra Yep https://orcid.org/0000-0002-0909-6120
Todd J. Henry https://orcid.org/0000-0002-9061-2865
Leonardo Paredes https://orcid.org/0000-0003-1324-0495
Wei-Chun Jao https://orcid.org/0000-0003-0193-2187

References

Abt, H. A., & Morgan, W. W. 1972, ApJL, 174, L131
Bailer-Jones, C. A. L., Rybizki, J., Fouesneau, M., et al. 2018, AJ, 156, 58
Baraffe, I., Homeier, D., Allard, F., et al. 2015, A&A, 577, A42
Barrado y Navascués, D., Stauffer, J. R., Briceño, C., et al. 2001, ApJS, 134, 103
Barrado y Navascués, D., Stauffer, J. R., & Jayawardhana, R. 2004, ApJ, 614, 386
Barrado, Y. N. D., Stauffer, J. R., & Patten, B. M. 2000, in ASP Conf. Proc. 198, Stellar Clusters and Associations: Convection, Rotation, and Dynamos, ed. R. Pallavicini et al. (San Francisco, CA: ASP), 269
Boudreault, S., & Bailer-Jones, C. A. L. 2009, ApJ, 706, 1484
Braes, L. L. E. 1962, BAN, 16, 297
Brandt, T. D., & Huang, C. X. 2015, ApJ, 807, 24
Bravi, L., Zari, E., Sacco, G. G., et al. 2018, A&A, 615, A37
Briceno, C., Calvet, N., Hernandez, J., et al. 2019, AJ, 157, 85
Buscombe, W. 1965, MNRAS, 129, 411
Butler, R. P., Marcy, G. W., Williams, E., et al. 1996, PASP, 108, 500
Cantat-Gaudin, T., Jordi, C., Vallenari, A., et al. 2018, A&A, 618, A93
Casey, A. R., Ruchti, G., Masseron, T., et al. 2016, MNRAS, 461, 3336
Cayrel, R. 1988, The Impact of Very High S/N Spectroscopy on Stellar Physics, Vol. 132 (Dordrecht: Kluwer), 345
Cummings, J. D., Deliyannis, C. P., Maderak, R. M., et al. 2017, AJ, 153, 128
D'Orazi, V., De Silva, G. M., & Melo, C. F. H. 2017, A&A, 598, A86
D'Orazi, V., & Randich, S. 2009, A&A, 501, 553
De Silva, G. M., D'Orazi, V., Melo, C., et al. 2013, MNRAS, 431, 1005
Deliyannis, C. P., Anthony-Twarog, B. J., Lee-Brown, D. B., et al. 2019, AJ, 158, 163
Deliyannis, C. P., Pinsonneault, M. H., & Duncan, D. K. 1993, ApJ, 414, 740
Dobbie, P. D., Lodieu, N., & Sharp, R. G. 2010, MNRAS, 409, 1002
Dodd, R. J. 2004, MNRAS, 355, 959
Drimmel, R., Bucciarelli, B., & Inno, L. 2019, RNAAS, 3, 79
Eastman, J., Gaudi, B. S., & Agol, E. 2013, PASP, 125, 83
Eggen, O. J. 1975, PASP, 87, 37
Eggen, O. J. 1983a, MNRAS, 204, 377
Eggen, O. J. 1983b, MNRAS, 204, 391
Eggen, O. J. 1991, AJ, 102, 2028
Esplin, T. L., & Luhman, K. L. 2019, AJ, 158, 54
Feinstein, A. 1961, PASP, 73, 410
Foster, D. C., Byrne, P. B., Hawley, S. L., et al. 1997, A&AS, 126, 81
Gaia Collaboration, Babusiaux, C., van Leeuwen, F., et al. 2018, A&A, 616, A10
Gagné, J., Mamajek, E. E., Malo, L., et al. 2018, ApJ, 856, 23
Gaidos, E., Mann, A. W., Rizzuto, A., et al. 2017, MNRAS, 464, 850
Gray, D. F. 1976, A Wiley-Science Publication (New York: Wiley)
Gray, D. F. 1992, CAS, 20, 1
Gutiérrez Albarrán, M. L., Montes, D., Gómez Garrido, M., et al. 2020, A&A, 643, A71
Hayes, C. R., & Friel, E. D. 2014, AJ, 147, 69
Jones, J., White, R. J., Boyajian, T., et al. 2015, ApJ, 813, 58
Lada, C. J., & Lada, E. A. 2003, ARA&A, 41, 57
Levato, H., Garcia, B., Lousto, C., et al. 1988, Ap&SS, 146, 361
Lindegren, L., Hernández, J., Bombrun, A., et al. 2018, A&A, 616, A2
Lodieu, N., Pérez-Garrido, A., Smart, R. L., et al. 2019, A&A, 628, A66
Luhman, K. L., & Esplin, T. L. 2020, AJ, 160, 44
Lyngå, G. 1962, ArA, 3, 65
Mann, A. W., Gaidos, E., Vanderburg, A., et al. 2017, AJ, 153, 64
Marsden, S. C., Carter, B. D., & Donati, J.-F. 2009, MNRAS, 399, 888
Merle, T., Van Eck, S., Jorissen, A., et al. 2017, A&A, 608, A95
Mermilliod, J.-C., Mayor, M., & Udry, S. 2009, A&A, 498, 949
Messina, S., Pizzolato, N., Guinan, E. F., et al. 2003, A&A, 410, 671
Newville, M., Stensitzki, T., Allen, D. B., et al. 2014, LMFIT: Non-Linear Least-Square Minimization and Curve-Fitting for Python, Zenodo, doi: 10.5281/zenodo.11813
Ochsenbein, F., Bauer, P., & Marcout, J. 2000, A&AS, 143, 23
Paredes, Leonardo A., Henry, Todd J., Quinn, Samuel N., et al. 2021, AJ, 162, 176
Paulson, D. B., & Yelda, S. 2006, PASP, 118, 706
Pecaut, M. J., & Mamajek, E. E. 2013, ApJS, 208, 9
Platais, I., Melo, C., Mermilliod, J.-C., et al. 2007, A&A, 461, 509
Quinn, S. N., & White, R. J. 2016, ApJ, 833, 173

Ragusa, E., Rosotti, G., Teyssandier, J., et al. 2018, MNRAS, 474, 4460
Randich, S., Aharpour, N., Pallavicini, R., et al. 1997, A&A, 323, 86
Randich, S., Bragaglia, A., Pastori, L., et al. 2005, Msngr, 121, 18
Randich, S., Pallavicini, R., Meola, G., et al. 2001, A&A, 372, 862
Randich, S., Primas, F., Pasquini, L., et al. 2002, A&A, 387, 222
Randich, S., Tognelli, E., Jackson, R., et al. 2018, A&A, 612, A99
Richer, H. B., Caiazzo, I., Du, H., et al. 2021, ApJ, 912, 165
Rolleston, W. R. J., & Byrne, P. B. 1997, A&AS, 126, 357
Simon, T., & Patten, B. M. 1998, PASP, 110, 283
Spina, L., Randich, S., Magrini, L., et al. 2017, A&A, 601, A70
Stauffer, J. R., Hartmann, L. W., Prosser, C. F., et al. 1997, ApJ, 479, 776
Tokovinin, A., Fischer, D. A., Bonati, M., et al. 2013, PASP, 125, 1336
Torres, C. A. O., Quast, G. R., Melo, C. H. F., et al. 2008, Handbook of Star Forming Regions, Vol. 2 (San Francisco: ASP), 757
Vesper, D. N., & Honeycutt, R. K. 1993, PASP, 105, 731
Wenger, M., Ochsenbein, F., Egret, D., et al. 2000, A&AS, 143, 9
Wevers, T., Hodgkin, S. T., Jonker, P. G., et al. 2016, MNRAS, 458, 4530
White, R. J., Gabor, J. M., & Hillenbrand, L. A. 2007, AJ, 133, 2524
Whiteoak, J. B. 1961, MNRAS, 123, 245
Wright, J. T., & Eastman, J. D. 2014, PASP, 126, 838
Wu, Z.-Y., Zhou, X., Ma, J., et al. 2009, MNRAS, 399, 2146
Yee, S. W., Petigura, E. A., & von Braun, K. 2017, ApJ, 836, 77
Zuckerman, B., Klein, B., & Kastner, J. 2019, ApJ, 887, 87